Remote Sensing of Environment 122 (2012) 106–116

Contents lists available at SciVerse ScienceDirect

Remote Sensing of Environment

journal homepage: www.elsevier.com/locate/rse

Quantifying forest cover loss in Democratic Republic of the Congo, 2000–2010, with Landsat ETM+ data

Peter V. Potapov [a,*], Svetlana A. Turubanova [a], Matthew C. Hansen [a], Bernard Adusei [a], Mark Broich [a], Alice Altstatt [b], Landing Mane [c], Christopher O. Justice [b]

[a] Geographic Information Science Center of Excellence, South Dakota State University, Brookings, SD 57007, USA
[b] University of Maryland College Park, Department of Geography, College Park, MD 20742, USA
[c] Observatoire Satellital des Forêts d'Afrique Centrale (OSFAC), Kinshasa, Democratic Republic of the Congo

ARTICLE INFO

Article history:
Received 2 May 2011
Received in revised form 27 July 2011
Accepted 6 August 2011
Available online 9 February 2012

Keywords:
Forest cover
Forest cover loss
Landsat
Congo

ABSTRACT

Forest cover and forest cover loss for the last decade, 2000–2010, have been quantified for the Democratic Republic of the Congo (DRC) using Landsat time-series data set. This was made possible via an exhaustive mining of the Landsat Enhanced Thematic Mapper Plus (ETM+) archive. A total of 8881 images were processed to create multi-temporal image metrics resulting in 99.6% of the DRC land area covered by cloud-free Landsat observations. To facilitate image compositing, a top-of-atmosphere (TOA) reflectance calibration and image normalization using Moderate Resolution Imaging Spectroradiometer (MODIS) top of canopy (TOC) reflectance data sets were performed. Mapping and change detection was implemented using a classification tree algorithm. The national year 2000 forest cover was estimated to be 159,529.2 thousand hectares, with gross forest cover loss for the last decade totaling 2.3% of forest area. Forest cover loss area increased by 13.8% between the 2000–2005 and 2005–2010 intervals, with the greatest increase occurring within primary humid tropical forests. Forest loss intensity was distributed unevenly and associated with areas of high population density and mining activity. While forest cover loss is comparatively low in protected areas and priority conservation landscapes compared to forests outside of such areas, gross forest cover loss for all nature protection areas increased by 64% over the 2000 to 2005 and 2005 to 2010 intervals.

1. Introduction

Tropical forests serve as a major carbon pool, storing the largest amount of carbon in living biomass of all terrestrial biomes (IPCC, 2000). Tropical forests are also the largest terrestrial reservoir of biological diversity, and provide a number of other important ecosystem services in shaping the human environment of tropical countries. The humid forests of Central Africa feature the second largest continuous tropical forest massif in the world, about half of which is located within the boundaries of the Democratic Republic of the Congo (DRC). Compared to other countries within Central Africa, the DRC features the highest area of annual forest cover loss (FAO, 2010). Forest cover loss intensity is a function of high population density (second highest in Central Africa after Cameroon) and the highest population growth rate within the region (CBFP, 2009). On the other hand, forest cover loss in the DRC is considerably less than other humid tropical countries such as Brazil or Indonesia (FAO, 2010; Hansen et al., 2010). DRC's relatively low forest loss can be explained by a lack of intensive industrial agriculture or forestry. Years of civil war and economic instability have hindered agro-industrial investment and development. The rural population of the country relies mainly on slash-and-burn subsistence agriculture techniques, and the timber harvest volumes (as of year 2007) within the DRC were the lowest compared to other Central African nations (CBFP, 2009).

While forest cover loss within the DRC is moderate, it is spatially pervasive. The expansion of human populations into previously intact areas, followed by forest fragmentation, forest conversion for slash-and-burn agriculture, mining operations, charcoal production, and poaching all deleteriously impact DRC's forest resources and the future sustainability of forest ecosystem services. The quantification of forest cover extent and change at the national scale is valuable for forest resource management, land use planning and conservation monitoring. However, such information is sparse or lacking for the DRC. Satellite imagery are the only viable data source currently available for the quantification of forest cover and loss within the DRC, given the vast extent of intact forest landscapes, lack of transportation infrastructure and political instability which limit data collection and forest mapping on the ground. An additional advantage of satellite monitoring is its independence from national administrations, allowing open publication of the mapping and monitoring results. This enhances overall transparency of forest information as it is immediately available to civil society, private industry and governments in support of science, conservation and other forest resource assessment and

* Corresponding author.
E-mail address: peter.potapov@hermes.geog.umd.edu (P.V. Potapov).

0034-4257/$ – see front matter
doi:10.1016/j.rse.2011.08.027

management applications. Recently, several projects' results were published on satellite forest cover and change estimates within Central Africa using sample-based (Achard et al., 2002; Duveiller et al., 2008; Hansen et al., 2010) and mapping approaches (Hansen et al., 2008; IES, 2008). Sample-based estimates were based on classified Landsat subsets selected using regular (Duveiller et al., 2008) or stratified sampling designs (Achard et al., 2002; Hansen et al., 2010). Both approaches, however, have problems with estimate precision due to the uneven distribution of change within forest landscapes (Tucker and Townshend, 2000). Moreover, only Hansen et al. (2010) provided forest cover and change estimates for the entire country, beyond humid tropical forest biome boundaries. The standard error for sample-based forest loss estimates within DRC was high, reaching 25% (Duveiller et al., 2008) to 100% (Hansen et al., 2010) of the estimated change area.

Concerning mapping methods, the typical fine scale of forest clearing in the DRC precludes area change estimation using coarse spatial resolution sensors such as MODIS. Finer spatial resolution data, such as that of the Landsat sensor, do allow for accurate forest cover change area measurement (Wulder, 1998). Landsat imagery has been the data source of choice for many tropical forest monitoring efforts (Broich et al., 2011; INPE, 2002; Killeen et al., 2007). The use of Landsat data for national-scale forest monitoring in DRC has been limited until recently due to the combined impacts of high data costs and persistent cloud cover. In January 2008, the U.S. Geological Survey (USGS) implemented a new Landsat Data Distribution Policy that provides Landsat data free of charge (Woodcock et al., 2008). Recent progress in automated Landsat data processing and mosaicing to produce cloud-free annual or epochal composite images (Broich et al., 2011; Hansen et al., 2008; Potapov et al., 2011; Roy et al., 2010) has enabled Landsat-based monitoring for large regions such as the DRC.

The objective of our study was to provide forest cover maps for the year 2000 and to map gross forest cover loss between 2000 and 2010 for the DRC. An exhaustive mining of the Landsat ETM+ archive was performed to map forest cover extent and loss. Our data processing and mapping algorithm was an evolution of the approach of Hansen et al. (2008), where data from MODIS are used to pre-process Landsat time-series images which are in turn used to characterize forest cover extent and loss. Our approach is based on a fully automated Landsat scene selection, per-pixel quality assessment and normalization algorithm. Individual Landsat images were used to derive multi-temporal metrics and multi-year composites which were integrated with MODIS time series data for regional-scale forest cover and change mapping.

The forest cover and monitoring results for 2000–2010 were compared with results from Hansen et al. (2008) for the 1990–2000 interval and analyzed to reveal generic patterns in forest cover loss dynamics within the country. We also estimated forest cover loss within the protected areas of the DRC, highlighting those experiencing elevated rates of habitat destruction. This analysis is a contribution to the United States Agency for International Development (USAID)-funded CARPE (Central Africa Regional Program for the Environment) project, a long-term initiative by USAID to address the issues of forest management, human livelihoods, and biodiversity loss in the Congo Basin forest zone (http://carpe.umd.edu). The study was performed in partnership with the non-governmental organization OSFAC (Observatoire satellital des forêts d'Afrique central), which works to provide satellite data and derived forest monitoring products to governments, civil society and other parties interested in the forest resources of the Congo Basin (http://osfac.net). Forest cover and change maps can be viewed and downloaded from the dedicated web site (http://congo.iluci.org/carpemapper/).

2. Data

2.1. Landsat data

To map forest cover and change, we employed the entire archive of Landsat ETM+ data for the DRC from 2000 to 2010 available at the USGS National Center for Earth Resources Observation and Science (EROS). A total of 8881 images having less than 50% cloud cover for any scene quarter according to image metadata for 120 Worldwide Reference System-2 (WRS2) path/rows covering the DRC were selected and downloaded. Only images processed as Level 1 terrain corrected (L1T) data by USGS EROS were used. For image quality assessment all reflective spectral bands (bands 1–5 and 7) together with the ETM+ thermal high gain channel denoted as band 62 were employed. Four bands (band 3–5 and 7) were normalized and included in the final image composites used to map forest cover type, extent and loss.

2.2. Ancillary data

A set of MODIS-derived metrics were used as a normalization target for Landsat image processing and were appended to Landsat inputs as additional metrics for the forest and change classification. MODIS metrics were produced from 2000 to 2009 10-year global Terra/MODIS 16-day composite data (MOD44C, collection 5) provided by the University of Maryland (Carroll et al., 2010). The MOD44C product consists of reflective bands 1–7 along with brightness temperature bands resampled to 250 m spatial resolution. To reduce the presence of clouds and shadows, the surface reflectance and brightness temperature values from observations with the lowest cloud probability over the 2000–2009 interval for each 16-day composite were selected. A set of annual metrics, defined following the approach of Hansen and DeFries (2004), was created from 23 16-day composite values. Metrics included mean reflectance for MODIS bands 1, 2, 6 and 7 for six 16-day intervals corresponding to the highest annual brightness temperature and highest NDVI composite values (total 8 metrics). MODIS spectral bands were chosen to correspond with Landsat bands 3, 4, 5, and 7. Reflectance values of 0–100% were scaled to 1–255 and stored as 8 bit data layers.

The Landsat imagery was appended with Shuttle Radar Topography Mission (SRTM) elevation and computed slope layers. The void-filled seamless SRTM data available from the CGIAR-CSI SRTM 90 m Database (http://srtm.csi.cgiar.org) were used. SRTM elevation data were resampled to the Landsat pixel grid.

3. Methods

3.1. Image processing

Landsat automatic image processing steps included: (1) image resampling, (2) conversion of raw digital values (DN) to top of atmosphere (TOA) reflectance, (3) cloud/shadow/water screening and quality assessment (QA), and (4) image normalization.

Landsat L1T images were reprojected from local UTM projections to the Sinusoidal projection (central meridian 20°E) and mapped to a predefined pixel grid using bilinear interpolation to facilitate further image compositing. The predefined pixel grid had a spatial resolution of 60 m to reduce false change detection due to residual sub-pixel misregistration effects (Townshend et al., 1992). To minimize differences in ETM+ sensor calibration, sun-earth distance and sun elevation, the raw image DN values were converted to TOA reflectance (for reflective bands) and brightness temperature (for band 62). We used the approach described in Chander et al. (2009) with coefficients taken from image metadata. TOA reflectance (0–100%) and brightness temperature values (240–320 K) were scaled to 1–255 and stored as 8 bit data layers.

For per-pixel QA assessment, a set of cloud, shadow and water detection models was used. The models correspond to a set of classification tree models (Breiman et al., 1984) derived from training data. To collect training data, 92 Landsat images were selected in different parts of the tropical forest zone, and each classified to land, water, cloud, and shadow classes. From these images, 1% samples were randomly selected and used to create the generalized classification tree models. Each model was applied per Landsat image, yielding cloud,

shadow and water class probability values. Based on these values a QA code was assigned to each pixel reflecting the probability of the pixel to be a land or water cloud-free observation, similar to the method described in Potapov et al. (2011).

Radiometric normalization was used in our algorithm to reduce reflectance variations between image dates due to atmospheric conditions and surface anisotropy. Bulk corrections for atmospheric effects can be made using the computationally simple dark-object subtraction (DOS) method (Chavez, 1988). A previous approach identified dark-object normalization targets from a MODIS-derived mature forest cover map (Hansen et al., 2008). While this relatively simple method has been shown to be sufficient for image normalization for regional-scale image mosaicing, it could only be implemented if a significant portion of the image scene is covered with the normalization target (Potapov et al., 2011). For Central Africa, the DOS normalization approach proposed by Hansen et al. (2008) relied on dense humid tropical forest cover as the dark target, making this method inappropriate for savanna and woodland regions. We modified this approach by using the MODIS surface reflectance aggregated from cloud-free observations from 10 years of data (see Section 2.2) as the normalization target. To normalize Landsat imagery, we calculated a mean bias between MODIS surface reflectance and Landsat TOA reflectance for each spectral band over the land area and used it to adjust Landsat reflectance values. To exclude the clouds, cloud shadows, and areas representing rapid land-cover change, only pixels with MODIS-Landsat reflectance difference below 0.05 were included in the normalization mask.

The estimated bias, however, is not constant within the Landsat scene due to the effect of surface anisotropy combined with variations in the viewing and solar geometries. While the best up-to-date developed approach for radiometric correction of Landsat surface anisotropy effect is to use an empirical bi-directional reflectance distribution function (BRDF) model (Danaher, 2002), a simpler linear model can be successfully implemented for relative image normalization (Hansen et al., 2008). The effect of surface anisotropy is pronounced across track and linearly correlated with scan angle. This effect has some variations between different land-cover types (Danaher, 2002) with tall vegetation (forests) having a higher slope of the regression compared to short vegetation and bare ground. We considered this variation to be negligible within the single Landsat scene. To simplify computation, the distance from the orbit ground track (calculated using adjacent Landsat scene center points) was used instead of scan angle. A simple linear regression between the MODIS-Landsat reflectance bias (y) and distance from orbit ground track (x) was estimated for each reflective band as:

$$y = a + bx \tag{1}$$

Derived slope (b) and intercept (a) of this linear regression were then used to correct band reflectance values within the entire Landsat image. Image normalization was performed independently for each spectral band and Landsat image (Fig. 1). For images having high cloud cover and/or low land fraction, a simple bias-adjustment correction was used to avoid incorrect regression estimation from few cloud-free land observations.

3.2. Image compositing

Several methods for dense coarse and medium spatial resolution image time-series analysis have been developed recently, including multi-date image compositing (Hansen et al., 2008; Holben, 1986; Roy et al., 2010), reflectance trend analysis (Kennedy et al., 2007) and multi-temporal metrics (DeFries et al., 1995; Hansen et al., 2003; Potapov et al., 2011). Our approach employs multi-date image compositing to generate start/end date image mosaics and multi-temporal metrics for analysis of reflectance variation within the analyzed time interval. Image compositing was performed independently for two 6-year time intervals: 2000–2005 and 2005–2010. To facilitate data processing, compositing was performed independently for a set of rectangular tiles consisting of 2000×2000 pixel grids (a total 205 tiles covering the DRC). The image compositing algorithm consisted of two stages: (1) QA analysis and "data pool" image date selection; and (2) multi-temporal metric and start/end date image composites generation.

To create a per-pixel set of cloud-free image observations, hereafter referred to as the "data pool", QA layers of all images overlapping within a particular composite tile were stacked in a single database. Our goal was to preferentially select images from the growing season as they are more appropriate for forest cover mapping than imagery captured during senescence or dormant periods (Tucker et al., 2004). Growing season boundaries were defined for each WRS2 path/row using MODIS-derived NDVI profiles. For northern woodlands, the growing season was defined from Julian day 321 of the current year to day 128 of the subsequent year; for southern savannas and woodlands, the growing season was defined from day 129 through 304; for humid tropical regions, the entire year was considered. To include information on image season for date preferential image selection, the QA codes were modified (by adding a second digit) for images acquired within the growing season. A set of criteria was designed to identify observations with the least cloud/shadow contamination to be included in the "data pool". First, permanent water pixels were selected as having a fraction of water-flagged observations for all non cloudy observations greater or equal to 50%. Next, for pixels with few growing season cloud/shadow free observations, search boundaries were extended first to out-of-season observation, then to observations with moderate cloud/shadow probabilities. After "data pool" pixels were selected, all other data (flagged as having higher cloud/shadow probability or out of season) were excluded from further processing. If no cloud/shadow free observations were found, pixels were mapped as "no data" and excluded from the analysis.

The "data pool" observations were used to create a set of spectral metrics representing reflectance variation within the growing season. The metrics are designed to capture a generic feature space that facilitates regional-scale mapping and have been used extensively with MODIS data in characterizing forest cover and croplands (Hansen et al., 2003; Pittman et al., 2010). Creating metrics using Landsat inputs is more complicated than with MODIS due to the increased variation in observation counts per pixel. The creation of the "data pool" facilitated their calculation. Three groups of per-band metrics were created: (1) reflectance values representing 6-year maximum, minimum and selected percentile values (10, 25, 50, 75 and 90% percentiles); (2) mean reflectance values for observations between selected percentiles (for the max–10%, 10–25%, 25–50%, 50–75%, 75–90%, 90%–max, min–max, 10–90%, and 25–75% intervals); and (3) slope of linear regression of band reflectance value versus image date over 6-year interval. Multi-temporal metrics were not used for visualization or interpretation, but were used for forest cover and change classification. Additional metrics included start/end date composites consisting of the earliest and latest observations as well as a composite of per-band median reflectance value for the 3 earliest/latest observations. This last metric was used in image interpretation for deriving classification training data sets.

3.3. Forest classification and change detection

Forest cover and forest types were mapped for circa year 2000. Bagged classification tree models (Breiman, 1996) were used to map forest/non-forest classes, and then to map primary humid tropical forests and secondary humid tropical forests classes within the generic forest mask. To build the classification tree model, an extensive forest/non forest training set was manually created by visual interpretation of the composite imagery representing the earliest cloud-free observation for 2000–2005 time interval (median image date September 2, 2000). Forest was defined as 30% or greater canopy cover for trees of

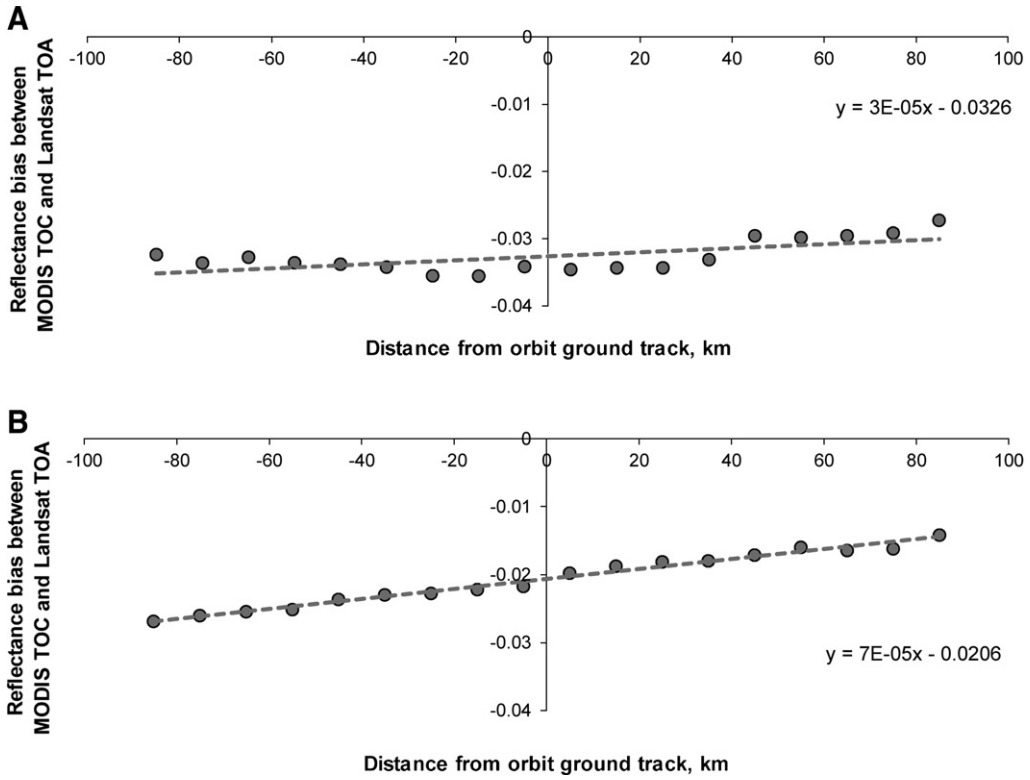

Fig. 1. Relationship between distance from estimated orbital ground track (negative values represent East side of the scene center, positive values represent West of center) and SWIR reflectance bias between Landsat TOA (band 5) and MODIS TOC (band 6) for images: A. Path 175, Raw 68 (located within dry tropical woodland biome), image date 04/19/2009. B. Path 175, Raw 60 (located within humid tropical forest biome), image date 02/1/2010. Slope and intercepts of the linear regression models were used to normalize the corresponding Landsat images. The mean bias values for each 10-km interval shown.

5 meters or more in height. A number of additional datasets, including freely available QuickBird images from GoogleEarth™ and expert information were used as reference materials to aid interpretation. The vast majority of image interpretation effort was focused on distinguishing savannas with tree canopy less than 30% from woodlands with a higher tree canopy density. The classification tree model relates manually interpreted training with the entire set of spectral metrics for the 2000–2005 time interval.

The primary humid tropical forest class was defined as mature humid tropical forest with greater than 60% canopy cover. This class was mapped separately within the generic forest mask using a manually created training set. Secondary forest was defined as regrowing forest with greater than 60% canopy cover. This class was mapped using multiple criteria, including geographic distribution, proximity to remain primary forest patches, tree composition and canopy density. To map secondary forests, a supervised classification model was created using a manually created training set. Woodland is defined as forest cover with greater than 30% and less than or equal to 60% canopy cover. After mapping primary and secondary humid tropical forest classes the remaining forest cover was assigned to the woodland class.

Gross forest cover loss from 2000 to 2005 was mapped within the resulting year 2000 forest mask, and forest cover loss 2005–2010 was mapped within the remaining forest area of 2005. Two sets of manually interpreted training sites were created using visual analysis of forest cover change for the 2000–2005 and 2005–2010 intervals, and two separate classification models were built upon these training data. The image composites for 2000, 2005 and 2010 years were used for visual interpretation of change training data, where the composite representing year 2005 was used as the endpoint for the 2000–2005 interval and as the start point for the 2005–2010 interval. The median composite dates are 9.02.2000, 5.07.2005, and 4.19.2010. All events resulting in stand replacement at the 60 meter pixel scale, including agriculture clearings (even followed by forest regrowth within the same time interval), logging, fire, flooding, and storm damage were mapped together and no discrimination between change types was made in our analysis.

3.4. Data analysis and comparison

After creating a forest cover and change map, we provided an analysis of forest and change distribution per administrative region using provincial boundaries provided by the World Resources Institute (WRI, 2010). Change dynamics were analyzed by calculating mean distances between pixels of forest clearing class and secondary forest class, year 2000–2005 clearings, and roads provided by WRI (2010). To analyze forest cover loss spatial pattern, a forest loss patch map was built using the 60 m spatial resolution forest cover loss map and an 8-neighboring pixel aggregation. To select the largest cities, we used the LandScan 2005 Global Population Database developed by Oak Ridge National Laboratory (Dobson et al., 2000). From the population grid, areas with population density above 1000 persons per km^2 and having an extent of more than 5 km^2 were selected resulting in 55 urban areas. To estimate deforestation related to cities, we summarized primary and woodland forest change areas within a 50 km radius of each selected urban area.

The officially designated nature protection area (PA) database provided by WRI (2010) was used for the analysis of PA system effectiveness and to highlight threatened areas. A buffer zone of 10 km was analyzed in addition to the PA area. While an existing nature PA serves as a formal basis for national conservation strategy within the DRC, several alternative options for area prioritization and conservation effort targeting were proposed by non-governmental organizations. These include, but are not limited to, the regionally-based approach proposed by the CARPE program to select priority landscapes for monitoring biodiversity, deforestation and other measures

of disturbance within the remaining intact forest zones of the Congo Basin (CBFP, 2009). We have used a DRC-wide subset from the CARPE priority landscapes to examine primary forest cover loss.

4. Results and discussion

4.1. Satellite data coverage

Our forest cover and change analysis was performed for the entire area of the DRC, with 99.6% of the surface area covered by cloud-free Landsat observations. Gaps due to persistent cloud cover in coastal areas exist, specifically 18% of Bas Congo province and 1.6% of Kinshasa province. The near complete cloud-free data coverage was possible because of large number of image observations processed per path/row. On average, 39 observations per WRS2 path/row were used to create composites and metrics for both the 2000–2005 and 2005–2010 epochs. This is significantly higher than the 5 observations per path/row used by Hansen et al. (2008) for the 1990–2000 interval. This research is the first Congo Basin study to be performed after the opening of the Landsat archive, enabling a more exhaustive mapping effort. For the common area between the previous and current studies, the new composite product had 0.16% missing data compared to 1.12% missing data of the Landsat composites developed by Hansen et al. (2008).

4.2. Forest cover

The total forest cover for the DRC was estimated to be 159,529.2 thousand hectares (kha). Primary humid tropical forests occupy 66% of total forest extent, secondary humid tropical forests 11%, and woodlands 23%. Our forest cover estimates are close to that provided by the Congo Basin Forest Partnership (CBFP, 2009) for the year 2008 (155,500 kha) as well as that of the FRA (FAO, 2010) for the year 2000 (157,249 kha). Our results showed a 1.4% overestimation compared to FAO FRA data and a 2.5% overestimation compared to CBFP data. The last difference could be explained by forest change from 2000 (the year of our assessment) to 2008. If we exclude total gross forest loss area from 2000 to 2010 from our year 2000 forest cover area, the estimate is within 1% of the CBFP figure. The overestimation is also found when comparing our estimate of primary humid tropical forests for 2000 (104,455.0 kha) to dense humid forests area estimated by the CBFP for 2008 (99,000 kha). While our national-scale forest cover estimates are similar to previously published data, our higher spatial resolution forest map allowed us to disaggregate these estimates to provincial (Table 1) and local scales.

4.3. Gross forest cover loss

The area of gross forest cover loss from 2000 to 2010 was estimated to be 3711.8 kha, or 2.3% of total forest area for year 2000. Of the total forest loss, 57% occurred within secondary humid forests, 29% within primary humid forests, and 14% within woodlands. The percent of forest loss per forest type varied, with the highest rate of forest loss in regrowing humid tropical forests (11.6%) and the lowest in mature humid tropical forests (1.0%). While forest cover loss in mature forests is lower than in regrowing forests, it has more significant impacts on forest structure and biodiversity. Clearing in secondary forests is part of a rotational slash-and-burn agriculture practice or, to a much lesser degree, industrial timber plantation rotation (such as logging in Eucalyptus plantations near Bankana, Kinshasa province). These activities lead to secondary forest regeneration. Clearing in primary forests, in contrast, represents the expansion of agriculture into heretofore intact forests with subsequent changes in floristic species composition, ecosystem dynamics, and consequent loss of faunal biodiversity. Clearing within woodlands comprised 1.4% of forest area and consisted principally of agricultural expansion areas.

Total gross forest cover loss area increased by 13.8% from the 2000–2005 to 2005–2010 interval. The greatest increase was detected within primary humid tropical forests, where forest area loss increased by almost a factor of two (by 91.1%). This increase in primary forest loss was due to the expansion of agriculture and correlates with high rates of population growth within the DRC (2.8% annual growth for year 2008; FAO, 2010). Forest loss also increased within woodlands by 63.3%, while for the secondary humid tropical forests the gross forest loss decreased by 18.9%. It is hard to speculate on this dynamic, however, for some regions of Congo, the ongoing war has led to the displacement of populations away from road networks and into interior forests (Draulans and Van Krunkelsven, 2002).

While the distribution of total forest loss area at the provincial scale reflected their forest cover area, the forest loss intensity was distributed unevenly and reflected areas with high population density and growth rates (Table 1). Two Northern provinces, Equateur and Orientale, are responsible for 44% of the total forest loss within the country and for 49% of the forest loss within primary humid tropical forests. The forest loss intensity is highest in Kinshasa province (11.4% of forest cover for year 2000), followed by Kasai-Occidental, Sud-Kivu and Kasai-Oriental provinces. Primary forest loss intensity was highest in Kinshasa (9.6%) and Bas-Congo (4.5%) followed by Kasai-Occidental, Sud-Kivu, Katanga and Kasai-Oriental provinces, while it was below the national mean in the northern provinces of Equateur and Orientale.

The average annual gross forest loss for the 2000–2010 interval was 371.2 kha/year (0.23% of forest cover for year 2000). The annual forest loss increased from 0.22% for 2000–2005 to 0.25% for 2005–2010. Our gross forest cover loss estimate is 16% higher compared to FAO's (2010) net forest loss estimate of 311 kha/year. FAO did not report change in forest cover loss dynamics from 1990 to

Table 1
Forest cover for year 2000 and forest cover loss for 2000–2010 (thousand ha) per DRC province. HT — Humid tropical forests.

Region	Percent of region area analyzed	Forest area, 2000				Forest cover loss, 2000–2005				Forest cover loss, 2005–2010			
		Total forest	HT primary	HT secondary	Woodlands	Total forest	HT primary	HT secondary	Woodlands	Total forest	HT primary	HT secondary	Woodlands
Bandundu	100.0	15,887.3	10,019.0	2858.8	3009.5	199.2	33.8	150.4	15.0	183.2	67.6	82.7	32.9
Bas-Congo	82.0	892.4	78.8	579.7	234.0	13.6	1.3	10.2	2.1	10.7	2.3	6.0	2.4
Equateur	100.0	35,453.4	31,225.7	3574.5	653.2	379.0	90.1	284.8	4.1	421.9	162.2	254.3	5.4
Kasai-Occidental	100.0	9570.5	6802.9	1823.5	944.1	223.9	52.8	161.3	9.8	234.8	110.4	105.2	19.2
Kasai-Oriental	100.0	9845.2	7881.0	1202.9	761.3	148.1	36.6	105.6	5.9	165.9	62.4	94.8	8.6
Katanga	100.0	25,725.5	621.7	273.6	24,830.2	140.6	3.5	6.7	130.4	232.2	5.3	6.4	220.5
Kinshasa	98.4	97.4	14.9	54.9	27.6	4.7	0.4	3.6	0.6	6.5	1.0	4.2	1.2
Maniema	100.0	9983.3	7720.9	1604.0	658.4	142.9	30.1	109.8	3.0	141.4	54.0	82.2	5.1
Nord-Kivu	99.8	4590.9	3595.6	784.5	210.9	38.0	10.0	23.5	4.5	48.3	26.4	19.9	2.0
Orientale	100.0	43,064.0	33,232.9	4850.1	4981.0	373.2	91.7	258.8	22.8	450.1	180.4	241.8	27.9
Sud-Kivu	99.9	4419.3	3261.7	686.6	471.0	72.6	16.3	53.4	2.9	81.0	28.5	49.2	3.3
DRC total	99.6	159,529.2	104,455.0	18,293.1	36,781.1	1735.8	366.6	1168.1	201.2	1975.9	700.7	946.8	328.5

2010. Our wall-to-wall change detection results for 2000–2005 interval is also higher then sample-based estimates of gross forest loss (200 kha/year) provided by Hansen et al. (2010).

The mean change patch area for both the 2000–2005 and 2005–2010 intervals is 1.4 ha. Such a small clearing patch area suggests that the local slash-and-burn agriculture practices are the predominant forest cover loss driver. Based on visual Landsat composite data examination, no major forest fires or windfall events were evident during the study period, with the exception of forest fires caused by repeated Nyamuragira volcano eruptions in Nord-Kivu. Industrial agriculture clearing practices are rare in the DRC. The largest continuous clearing was detected at the southern edge of the humid tropical forest in Kasai-Orientale province, 40 km from the city of Mbuji-Mayi. A total area of 5.6 kha was contiguously cleared, with 1.1 kha cleared between 2000 and 2005, and remaining 4.5 kha cleared after 2005.

Within humid tropical forests, clearing patterns generally form buffers around the secondary forest belts due to the nearly continuous distribution of the rural population along roads (Fig. 2A). Within woodlands clearings often form circles around cities and villages (Fig. 2B), and are otherwise distributed along boundaries of open savannas and woodlands near settlements or roads. Since forest clearings are expanding within intact forest areas, the distance from roads or secondary forests increased for clearings from the 2005–2010 interval compared to the 2000–2005 interval. The mean distance from roads for all 60 m forest cover loss pixels was 4.4 km for 2000–2005 and 4.5 km for 2005–2010. Within humid tropical forests, the clearing expansion is more pronounced: the mean distance from primary forest clearing to the closest pixel of secondary forest was 335 m for 2000–2005 interval and increased to 437 m for the 2005–2010 interval.

Clearings from 2005 to 2010 are located near clearings from 2000 to 2005. The mean distance for all cleared pixels for the 2005–2010 interval to the closest pixels from 2000 to 2005 interval was 404 m. This distance may be longer, however, with the maximum detected speed of agriculture expansion from rural areas into intact forest areas equaling 1 km per year.

Most of the DRC population (about 66% according to FAO, 2010) is rural, and subsistence farming and consequent forest clearing is co-located with local population centers. The remaining population is within urban centers where in addition to agriculture, charcoal production is a major driver of forest cover loss. A third change dynamic is mining, which is done both formally and informally. Informal hotspots of mining are evident within a number of intact forest zones.

We provided an analysis of forest cover loss intensity within 50-km buffer areas of 55 selected major urban centers (Fig. 3). Cover loss within primary humid tropical forests and woodlands within all buffer zones was estimated to be 33% of the total forest cover loss for these categories of forests for the 2000–2010 interval. Our result shows that the most intensive clearings occur near towns located on the eastern and southern borders of the humid tropical forest zone, along the Congo River, and in southeastern woodland areas. Forest loss is lower within savanna areas and in the north-west of Equateur province. Forest loss was also low within wetland forest areas in Equateur and Bandundu provinces. Intensive forest loss areas are co-located with areas rich in metal deposits and diamonds, especially near large industrial (Tshikapa, Mbuji-Mayi, Kolwezi, Lubumbashi) and artisanal (Kisangani, Beni, Buta) mining areas. The intensive forest loss in Nord-Kivu province (Beni, Butembo) along the boundaries of Virunga National Park has been a major concern for forest conservation and is related to ongoing regional political unrest. Nearly all urban areas experienced increased forest clearing from 2000–2005 to 2005–2010.

The common area of analysis for this study and that of Hansen et al. (2008) covered a large portion of the humid tropical zone. Within the common area of analysis, the total forest cover loss for 1990–2000 intervals was estimated as 1.25% of study area, compared to 1.89% for the 2000–2010 interval, indicating a substantial decadal increase in forest loss (34%). Visual comparison of these datasets shows rapid expansion of agriculture areas within primary forests during the two-decade interval (Fig. 4). The comparison results are not reliable, however, due to differences in image classification methodology and input data richness.

4.4. Forest cover loss within protected areas and priority landscapes

The percentage of forest cover loss within primary humid tropical forests and woodlands was used as a main parameter to assess forest protection effectiveness within PAs. The mean percent of primary forest loss within protected areas was 0.4%, more than two times lower than the national average of 1.1% (Fig. 5). Forest loss was lower than the national average for 6 out of 7 National Parks (NP). The highest forest cover loss was observed within hunting reserves located on the

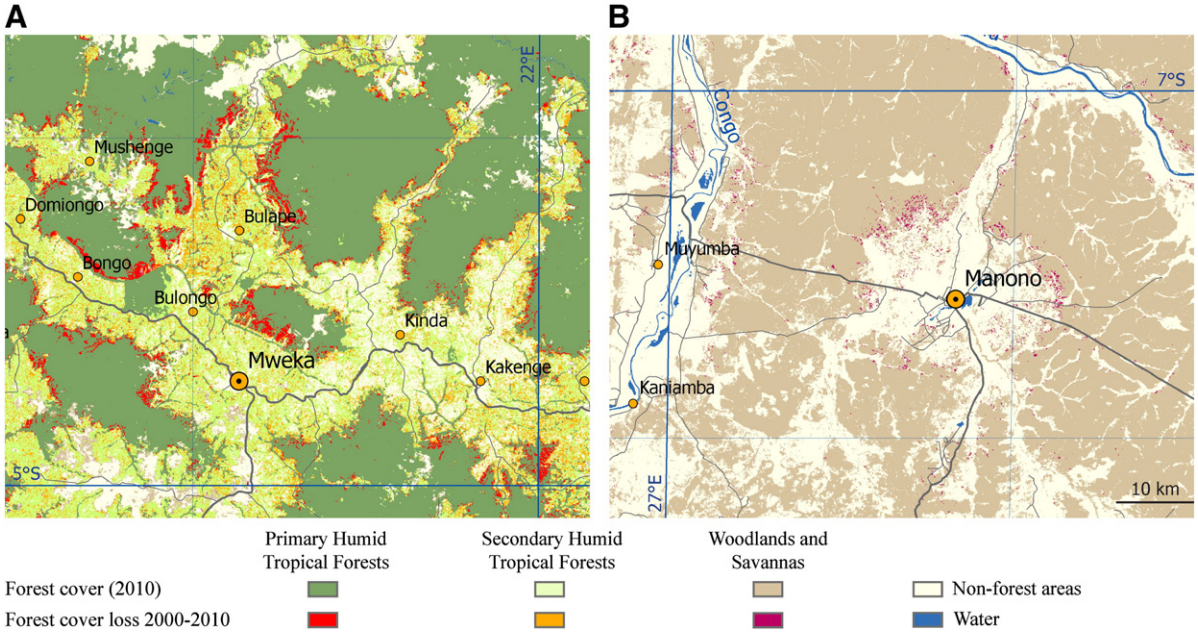

Fig. 2. Forest cover loss patterns: A. Within a humid tropical forest zone (Kasai-Occidental province); B. Within a woodland zone (Katanga province).

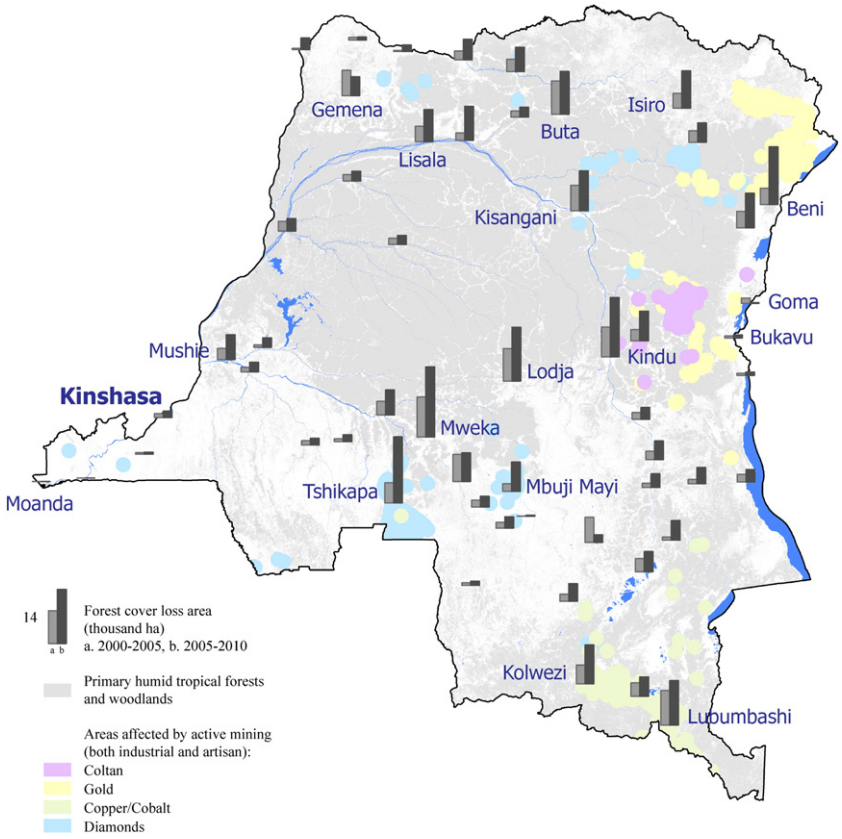

Fig. 3. Forest cover loss area 2000–2010 (thousand ha) within primary humid tropical forests and woodlands within a 50 km radius around selected major urban areas. Mining permit data for year 2010 were provided by the World Resources Institute.

boundary of humid tropical forests and savannas, and also close to the large mining centers of Lubumbashi and Kolwezi, where forest cover loss within several PAs was close to 5% for the last decade. While some PAs do not show signs of intensive forest disturbance, they often are adjacent to intensively cleared areas. The mean forest loss within 10-km buffers around all PAs was 0.9%, close to the national average. For example, forest cover loss in the 10-km buffer around Okapi Natural Reserve was 4 times higher compared to forest loss intensity within the Reserve. The highest differences between PA and buffer area forest loss estimates were found for Upemba and Kundelungu NPs located in the vicinity of large mining areas in Katanga Province. Gross forest cover loss increased by 64% between the 2000–2005 and 2005–2010 intervals for all PAs. The highest increase was detected within Lake Upemba and Kundelungu NPs. For PAs in northern and central regions, i.e. Salonga and Garamba NPs, increase was moderate, and for large PAs in Nord-Kivu and Sud-Kivu provinces (Virunga, Maiko and Kahuzi-Bienga NPs) a substantial reduction of forest clearing was detected.

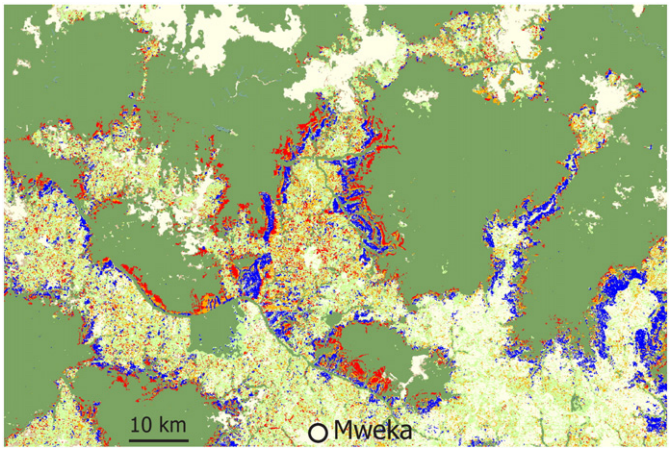

Fig. 4. Expansion of clearings within areas of primary humid tropical forests (Kasai-Occidental province, near Mweka). Blue — clearings 1990–2000, orange — clearings 2000–2005, red — clearings 2005–2010.

The high forest cover loss which occurred in Virunga National Park over the decade is unique. Forest loss within the Park is mostly connected with agriculture expansion and charcoal production, with the largest patch of contiguous deforestation near Beni (Fig. 6). A lesser, natural driver of change is related to the eruptions of the Nyamuragira volcano. The overall human-caused forest cover loss in Virunga NP is 0.87% for the decade, with a 48% decrease from 2000 to 2005 compared to 2005–2010. Regardless, Virunga NP remained one of the most threatened natural protection areas in the country, with the highest forest cover loss rate among all national parks, both within park limits and on adjacent territory.

Our results for the CARPE landscapes are similar to those obtained for PAs (Fig. 7). The mean forest loss area for the CARPE priority forest landscapes (0.6%) is half the national average. The highest forest cover loss of 2.6% was found in the Virunga landscape. However, Virunga forest cover loss intensity was stable during the last decade while forest clearing intensity grew rapidly for landscapes within Nord-Kivu and Sud-Kivu provinces. The Ituri-Epulu-Aru forest landscape experienced the highest, almost three-fold gain in forest cover loss, mostly due to agriculture expansion near Beni. The forests surrounding lakes Tumba and Tele near the western boundary of the DRC also experienced high rates of forest cover loss that nearly doubled over the last 5 years. Landscapes in the central part of the Congo basin experienced low forest clearing rates and moderate increases during the study period.

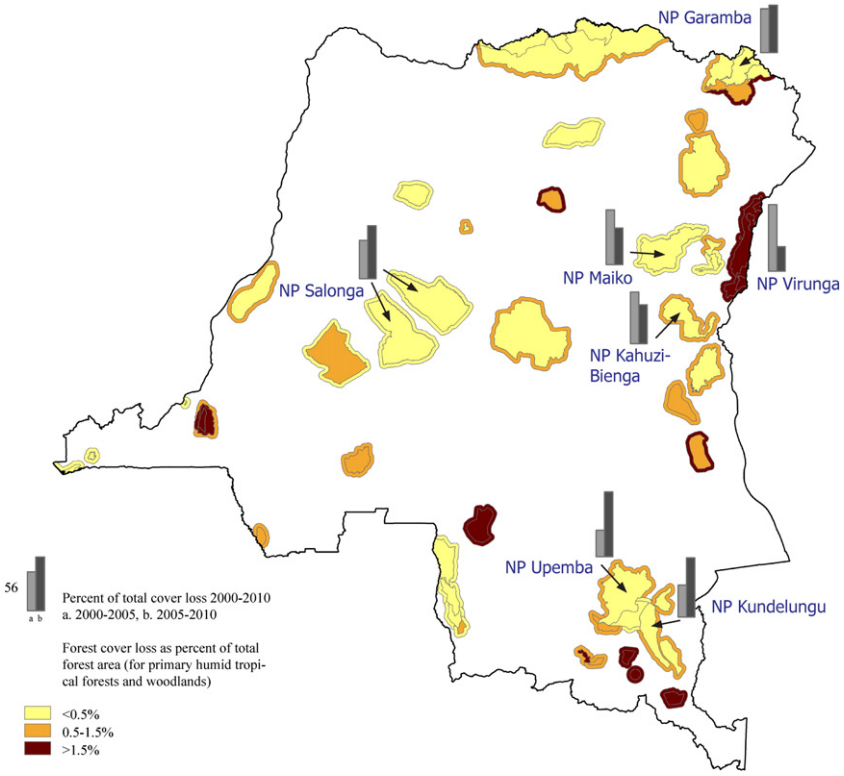

Fig. 5. Forest cover loss, 2000–2010, within officially designated nature protection areas and adjacent 10-km buffer zones. Percent of total forest cover loss for each 5-year interval is shown for National Parks. Only forest cover loss within primary humid tropical forests and woodlands were used for analysis.

5. Discussion

The availability of the entire Landsat archive at no cost provided data coverage of 99.6% of the entire nation. Cloud-affected areas were geographically concentrated within the coastal zone of Bas-Congo province. This limitation is not related to insufficient acquisitions (Arvidson et al., 2001). For example, within a persistently cloud-contaminated coastal scene (WRS2 path 183, row 64), 82% of all possible acquisitions were recorded during 2010. From these acquisitions, only 2 had metadata cloud cover less than 50% and included in our compositing procedure. Increasing cloud cover thresholds for scene selection in coastal regions could increase cloud-free observation counts for this region. Another important improvement would be to acquire Landsat 5 data over the region to complement the Landsat 7 archive. Currently, the western provinces of the DRC (Bas-Congo, Kinshasa and, partly, Bandundu) are located outside the area covered by regional Landsat 5 receiving stations (USGS, 2011). Adding a ground receiving station that covered the cloud-affected Central African coastal region is critically important for future forest monitoring. Our Landsat 7 archive mining results also suggested that single-sensor architecture of the future Landsat program (Wulder et al., 2011) would not be able to provide adequate data volumes for forest mapping and monitoring in areas of persistent cloud cover. A constellation of sensors with similar spectral and spatial resolutions, but varying overpass time and orbital cycle, is needed to provide sufficient data for forest monitoring in tropical regions.

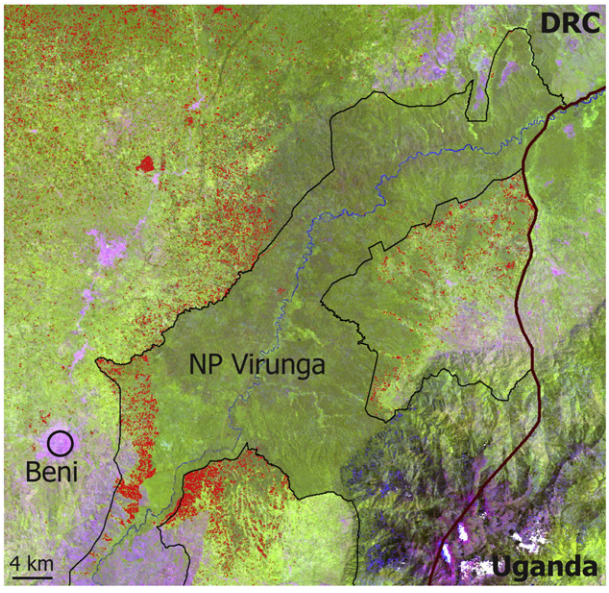

Fig. 6. Forest clearings 2000–2010 (shown in red) within Northern part of the Virunga National Park.

The atmospheric correction of Landsat-derived TOA reflectance data using actual (or extracted from the imagery) atmospheric parameters and 6S radiative transfer code is a state-of-the art method (Masek et al., 2006) that should be implemented for obtaining consistent surface reflectance. However, this method requires large amounts of ancillary time-synchronous atmospheric data. Simple normalization techniques for TOA reflectance correction using radiometrically consistent sets of moderate spatial resolution data have been developed and tested to create image composites over large regions (Gao et al., 2010; Olthof et al., 2005). Our methods rely on the correlation between Landsat TOA and MODIS TOC reflectance, the latter collected from the best cloud-free observations over several years of data. The MODIS-to-Landsat reflectance comparison for image normalization was performed only within the land mask, and a reflectance difference threshold was used to avoid areas of fast land-cover or phenological change. The comparison of obtained reflectance values from Landsat and MODIS data composites (Fig. 8 and 9) illustrates good correlation between the datasets.

Within our decision tree change detection model, the start/end date composites played the most important role, with 53% of total

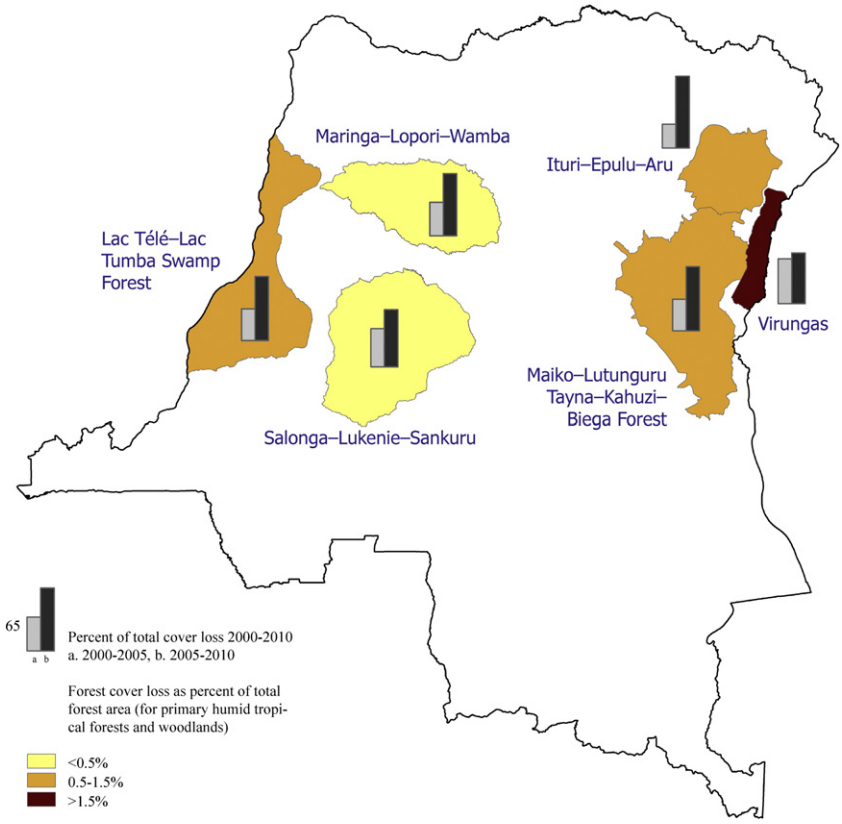

Fig. 7. Forest cover loss 2000–2010 and percent of total forest cover loss for each 5-year interval within CARPE landscapes. Only forest cover loss within primary humid tropical forests and woodlands were used for this analysis.

deviance decrease within the model attributed to start/end composites and their differences. From the spectral metrics, the slope of linear regression of band reflectance value versus image date and the maximum band reflectance value over the 6-year interval were the most important inputs, contributing 9% and 5% deviance decrease respectively. From the ancillary data appended to the composites, MODIS metrics were responsible for 11% and SRTM elevation and slope for 4% deviance decrease.

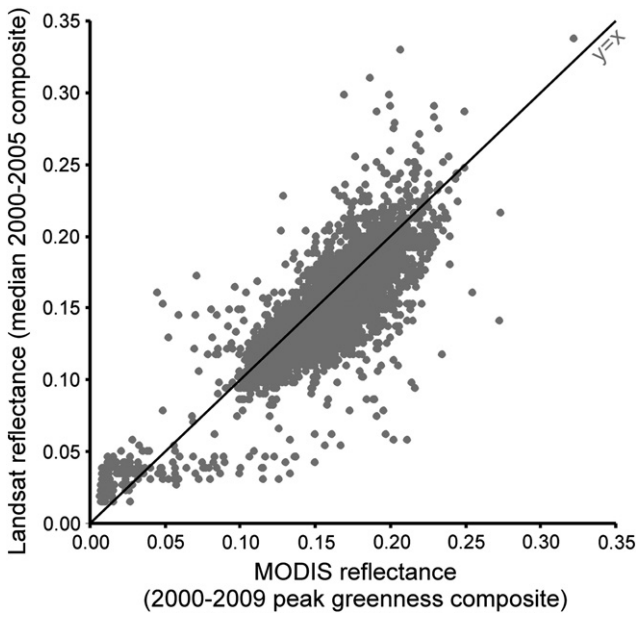

Fig. 8. Landsat SWIR 1550–1750 nm band vs. MODIS SWIR 1628–1652 nm band spectral reflectance. Landsat reflectance represents median MODIS-based calibrated reflectance value from all cloud-free observations for 2000 to 2005. MODIS reflectance represents mean TOC reflectance value for 6 16-day intervals with the highest NDVI. The 16-day interval values were collected from the least cloud contaminated observations from 2000 to 2009.

In the current implementation of our national-scale forest monitoring algorithm, forest gain has not been mapped. While some clearing of forest cover leads to the establishment of secondary savannas, most agricultural practices result in abandonment and the subsequent establishment of secondary forest cover. As a result, forest gain area could be comparable to forest loss, especially given the fact that permanent industrial agriculture is rare or absent within forest areas of the DRC.

6. Conclusion

Landsat-based forest cover and change mapping using supervised expert-driven classification is a well established and accepted methodology, and has been implemented for regional-scale forest cover mapping and monitoring of the Congo basin (Duveiller et al., 2008; Hansen et al., 2008). Reported accuracies for expert-driven Landsat-based forest cover change detection range between 75% and 91% (Coppin and Bauer, 1994; Saksa et al., 2003). The comparison of our national-scale estimates with forest cover and change estimates provided by other sources showed agreement among the various existing estimates. In our research, the spatial accuracies of forest cover and change detection have not been rigorously validated due to a lack of high spatial resolution imagery and field data over the forests of the DRC. The lack of national-scale validation data for the 2000–2010 interval is a reality for this environment. During the first half of the past decade the country suffered from a civil war that precluded the collection of national-scale ground truth data such as forest inventory information. High spatial resolution data were also not collected on a regular basis and are problematic for change detection validation due to frequent cloud coverage. A future implementation of our approach

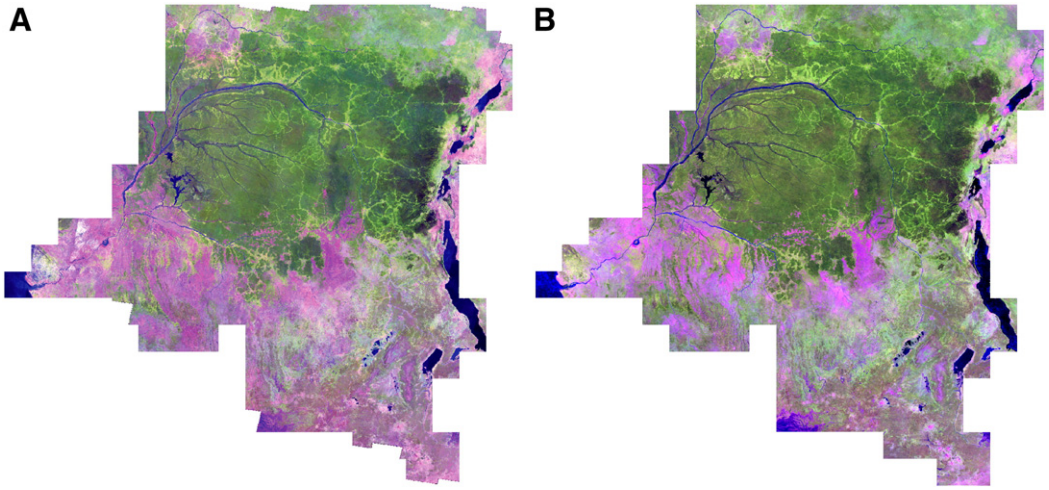

Fig. 9. A. Landsat median spectral reflectance from 2000 to 2005 composite. Color composite: Red — Landsat band 5 (SWIR); Green — Landsat band 4 (NIR); Blue — Landsat band 3 (Red). B. MODIS mean spectral reflectance from 2000 to 2009 peak greenness composite. Color composite: Red — MODIS band 6 (SWIR); Green — MODIS band 2 (NIR); Blue — MODIS band 1 (Red).

could be validated using a series of high spatial resolution data sets, acquired with the express purpose of forest change mapping validation. Because our results reveal that forest cover loss events are usually co-located with previously cleared areas and secondary forests, our current map product could be used for targeting samples of fine-scale imagery and used within a national-scale validation protocol. In this way, a consistent sampling database for a 2010–2015 mid-decadal change product validation could be established.

Large area medium spatial resolution land cover products such as the one developed in this study are made possible due to several recent advances in data policy and processing: (1) the global availability of free-of-charge terrain-corrected medium spatial resolution Landsat data; (2) improved high-performance computing for processing large volumes of remotely sensed data; (3) advances in the implementation of automated per pixel cloud/shadow detection and radiometric correction approaches; and (4) resulting large area image composites and multi-temporal metrics used as inputs to forest cover mapping and monitoring. While many challenges remain, including possible gap in future image availability and insufficient observation frequency, the approaches presented in this paper could be used in any tropical country. The technical ability for RS-based monitoring, however, does not solve the environmental problems in tropical regions. First, only several components of the ecosystem health can be monitored from space. Other components such as biodiversity threats from overhunting or chemical pollution caused by mining activities require a set of in situ measurements. Second, for most developing countries, the lack or weakness of governmental control on natural resources exploitation and political and economic instability prevents the efficient use of monitoring products in maintaining the ecosystem services of intact and/or protected areas. While our study showed some positive signs of effective forest conservation, i.e. the relatively low forest cover loss for most national parks and the decrease of forest clearing in the highly vulnerable Virunga NP, results also captured a high forest cover loss increase from 2000–2005 to 2005–2010. Other studies (Endamana et al., 2010) highlighted that there was little change in conservation indicators in Congo basin over the last decade. Moreover, the persistent armed conflicts in Central Africa coupled with the global economic downturn started in 2008 increased threats from illegal harvesting, poaching, artisanal mining and agriculture clearing expansion (Draulans and Van Krunkelsven, 2002; Endamana et al., 2010). The in-depth analysis of social drivers of forest cover change and the integration of forest monitoring methods into national natural resource management systems and international conservational initiatives are important future steps for national-scale monitoring activities.

Acknowledgments

This research was performed with support from the NASA Land Use Land Cover Change Program and the United States Agency for International Development (USAID) through the CARPE program (NASA grants NNX08AL99G and NNX09AD26G).

References

Achard, F., Eva, H. D., Stibig, H. J., Mayaux, P., Gallego, J., Richards, T., & Malingreau, J. P. (2002). Determination of deforestation rates of the world's humid tropical forests. *Science*, *297*, 999–1002.

Arvidson, T., Gasch, J., & Goward, S. N. (2001). Landsat 7's long-term acquisition plan — An innovative approach to building a global imagery archive. *Remote Sensing of Environment*, *78*, 13–26.

Breiman, L. (1996). Bagging predictors. *Machine Learning*, *24*, 123–140.

Breiman, L., Friedman, J. H., Olshen, R. A., & Stone, C. J. (1984). *Classification and regression trees*. Monterey, California: Wadsworth and Brooks/Cole.

Broich, M., Hansen, M. C., Stolle, F., Potapov, P. V., Margono, B. A., & Adusei, B. (2011). Remotely sensed forest cover loss shows high spatial and temporal variation across Sumatera and Kalimantan, Indonesia 2000–2008. *Environmental Research Letters*, *6*/*1*, doi:10.1088/1748-9326/6/1/014010.

Carroll, M., Townshend, J. R. G., Hansen, M. C., DiMiceli, C., Sohlberg, R., & Wurster, K. (2010). Vegetative cover conversion and vegetation continuous fields. In B. Ramachandran, C. Justice, & M. Abrams (Eds.), *Land remote sensing and global environmental change: NASA's EOS and the science of ASTER and MODIS*. New York: Springer.

CBFP (Congo Basin Forest Partnership) (2009). *The forests of the Congo Basin — State of the Forest 2008*. Luxembourg: Publications Office of the European Union, doi: 10.2788/32259.

Chander, G., Markham, B. L., & Helder, D. L. (2009). Summary of current radiometric calibration coefficients for Landsat MSS, TM, ETM+, and EO-1 ALI sensors. *Remote Sensing of Environment*, *113*, 893–903.

Chavez, P. S. (1988). An improved dark-object subtraction technique for atmospheric scattering correction of multispectral data. *Remote Sensing of Environment*, *24*, 459–479.

Coppin, P. R., & Bauer, M. E. (1994). Processing of multitemporal Landsat TM imagery to optimize extraction of forest cover change features. *IEEE Transactions on Geoscience and Remote Sensing*, *32*, 918–927.

Danaher, T. J. (2002). An empirical BRDF correction for Landsat TM and ETM + imagery. *Proceedings of the 11th Australasian Remote Sensing and Photogrammetry Conference, Brisbane, Australia* September 2002.

DeFries, R., Hansen, M., & Townshend, J. (1995). Global discrimination of land cover types from metrics derived from AVHRR pathfinder data. *Remote Sensing of Environment*, *54*, 209–222.

Dobson, J. E., Bright, E. A., Coleman, P. R., Durfee, R. C., & Worley, B. A. (2000). LandScan: A global population database for estimating populations at risk. *Photogrammetric Engineering and Remote Sensing*, *66*, 849–857.

Draulans, D., & Van Krunkelsven, E. (2002). The impact of war on forest areas in the Democratic Republic of Congo. *Oryx*, *36*(1), 35–40.

Duveiller, G., Defourny, P., Desclee, B., & Mayaux, P. (2008). Deforestation in Central Africa: Estimates at regional, national and landscape levels by advanced processing of systematically-distributed Landsat extracts. *Remote Sensing of Environment*, *112*, 1969–1981.

Endamana, D., Boedhihartono, A. K., Bokoto, B., Defo, L., Eyebe, A., Ndikumagenge, C., Nzooh, Z., Ruiz-Perez, M., & Sayer, J. A. (2010). A framework for assessing conservation and development in a Congo Basin Forest Landscape. *Tropical Conservation Science*, *3*(3), 262–281.

FAO [Food and agriculture organization of the United Nations] (2010). *Global forest resources assessment 2010.* Rome: UNFAO.

Gao, F., Masek, J. G., Wolfe, R. E., & Huang, C. (2010). Building a consistent medium resolution satellite data set using moderate resolution imaging spectroradiometer products as reference. *Journal of Applied Remote Sensing*, *4*, doi:10.1117/1.3430002.

Hansen, M., Stehman, S., & Potapov, P. (2010). Quantification of global gross forest cover loss. *Proceedings of the National Academy of Sciences of the Unites States of America*, *107*(19), 8650–8655.

Hansen, M. C., & DeFries, R. S. (2004). Detecting long term global forest change using continuous fields of tree cover maps from 8 km AVHRR data for the years 1982–1999. *Ecosystems*, *7*, 695–716.

Hansen, M. C., DeFries, R. S., Townshend, J. R. G., Carroll, M., Dimiceli, C., & Sohlberg, R. A. (2003). Global percent tree cover at a spatial resolution of 500 meters: First results of the MODIS vegetation continuous fields algorithm. *Earth Interactions*, *7*, doi:10.1175/1087-3562.

Hansen, M. C., Roy, D. P., Lindquist, E., Adusei, B., Justice, C. O., & Altstatt, A. (2008). A method for integrating MODIS and Landsat data for systematic monitoring of forest cover and change and preliminary results for Central Africa. *Remote Sensing of Environment*, *112*, 2495–2513.

Holben, B. (1986). Characteristics of maximum-value composite images from temporal AVHRR data. *International Journal of Remote Sensing*, *7*, 1417–1434.

IES [Institute for Environmental Security] (2008). *Mining, forest change and conflict in the Kivus, eastern Democratic Republic of Congo.* The Hague: IES.

INPE [Instituto Nacional de Pesquisas Espaciais] (2002). Deforestation estimates in the Brazilian Amazon. São José dos Campos: INPE. Available at. http://www.obt.inpe.br/prodes/.

IPCC [Intergovernmental Panel on Climate Change] (2000). *Land use, land-use change, and forestry. IPCC.* .

Kennedy, R. E., Cohen, W. B., & Schroeder, T. A. (2007). Trajectory-based change detection for automated characterization of forest disturbance dynamics. *Remote Sensing of Environment*, *110*, 370–386.

Killeen, T. J., Calderon, V., Soria, L., Quezada, B., Steininger, M. K., Harper, G., Solorzano, L. A., & Tucker, C. J. (2007). Thirty years of land-cover change in Bolivia. *Ambio*, *36*(7), 600–606.

Masek, J. G., Vermote, E. F., Saleous, N. E., Wolfe, R., Hall, F. G., Huemmrich, K. F., Gao, F., Kutler, J., & Lim, T. -K. (2006). A Landsat surface reflectance dataset for North America, 1990–2000. *IEEE Geoscience And Remote Sensing Letters*, *3*(1), 68–72.

Olthof, I., Butson, C., Fernandes, R., Fraser, R., Latifovic, R., & Orazietti, J. (2005). Landsat ETM+ mosaic of northern Canada. *Canadian Journal of Remote Sensing*, *31*(5), 412–419.

Pittman, K., Hansen, M. C., Becker-Reshef, I., Potapov, P. V., & Justice, C. O. (2010). Estimating global cropland extent with multi-year MODIS data. *Remote Sensing*, *2*, 1844–1863.

Potapov, P., Turubanova, S., & Hansen, M. C. (2011). Regional-scale boreal forest cover and change mapping using Landsat data composites for European Russia. *Remote Sensing of Environment*, *115*, 548–561.

Roy, D. P., Ju, J., Kline, K., Scaramuzza, P. L., Kovalskyy, V., Hansen, M. C., Loveland, T. R., Vermote, E. F., & Zhang, C. (2010). Web-enabled Landsat Data (WELD): Landsat ETM+ composited mosaics of the conterminous United States. *Remote Sensing of Environment*, *114*, 35–49.

Saksa, T., Uuttera, J., Kolstrom, T., Lehikoinen, M., Pekkarinen, A., & Sarvi, V. (2003). Clear-cut detection in boreal forest aided by remote sensing. *Scandinavian Journal of Forest Research*, *18*, 537–546.

Townshend, J. R. G., Justice, C. O., Gurney, C., & McManus, J. (1992). The impact of misregistration on change detection. *IEEE Transactions on Geoscience and Remote Sensing*, *30*, 1054–1060.

Tucker, C. J., Grant, D. M., & Dykstra, J. D. (2004). NASA's global orthorectified Landsat data set. *Photogrammetric Engineering and Remote Sensing*, *70*, 313–322.

Tucker, C. J., & Townshend, J. R. G. (2000). Strategies for monitoring tropical deforestation using satellite data. *International Journal of Remote Sensing*, *21*, 1461–1471.

USGS [U.S. Geological Survey] (2011). International Ground Station (IGS) network. Available at. http://landsat.usgs.gov/about_ground_stations.

WRI [World Resources Institute] (2010). *Atlas forestier interactif de la République Démocratique du Congo — version 1.0.* Washington, D.C: World Resources Institute.

Woodcock, C. E., Allen, R., Anderson, M., Belward, A., Bindschadler, R., Cohen, W., Gao, F., Goward, S. N., Helder, D., Helmer, E., Nemani, R., Oreopoulos, L., Schott, J., Thenkabail, P. S., Vermote, E. F., Vogelmann, J., Wulder, M. A., Wynne, R., & Team, L. S. (2008). Free access to Landsat imagery. *Science*, *320*, 1011.

Wulder, M. (1998). Optical remote-sensing techniques for the assessment of forest inventory and biophysical parameters. *Progress in Physical Geography*, *22*, 449–476.

Wulder, M. A., White, J. C., Masek, J. G., Dwyer, J., & Roy, D. P. (2011). Continuity of Landsat observations: Short term considerations. *Remote Sensing of Environment*, *115*, 747–751.